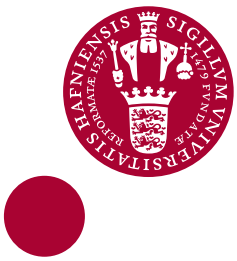

Coulomb-interaction-induced Majorana edge modes in nanowires

Li, Tommy; Burrello, Michele; Flensberg, Karsten

Published in:
Physical Review B

DOI:
10.1103/PhysRevB.100.045305

Publication date:
2019

Document version
Publisher's PDF, also known as Version of record

Coulomb-interaction-induced Majorana edge modes in nanowires

Tommy Li,[1] Michele Burrello,[1,2] and Karsten Flensberg[1]
[1]*Center for Quantum Devices, Niels Bohr Institute, University of Copenhagen, DK-2100 Copenhagen, Denmark*
[2]*Niels Bohr International Academy, Niels Bohr Institute, University of Copenhagen, DK-2100 Copenhagen, Denmark*

(Received 3 October 2018; published 11 July 2019)

We show that Majorana edge modes appear in a strongly correlated phase of semiconducting nanowires with discrete rotational symmetry in the cross section. These modes exist in the absence of spin-orbit coupling, magnetic fields, and superconductivity. They appear purely due to the combination of the three-dimensional Coulomb interaction and orbital physics, which generates a topological gap in one sector of the excitation spectrum as well as a topological ground-state degeneracy. The gap can be comparable in magnitude to the topological superconducting gap in other solid-state candidate systems for Majorana edge modes and may similarly be probed via tunnel spectroscopy.

DOI: 10.1103/PhysRevB.100.045305

I. INTRODUCTION

The quantum engineering of Majorana modes is one of the pinnacles of the study of topological phases of matter. In condensed-matter systems, these modes are fermionic quasiparticles equal to their own charge conjugates and thus a counterpart of the Majorana fermions proposed as elementary particles. Majorana modes were first predicted in two-dimensional p-wave superfluids [1] and superconductors [2], but their peculiar nonlocal behavior was fully understood only after they were demonstrated to exist as zero-energy modes in one-dimensional (1D) topological superconductors [3]. Following suggestions that a p-wave superconducting phase could be engineered in semiconductor nanowires using a combination of proximitization to a conventional s-wave superconductor [4,5], the native spin-orbit interaction in the semiconductor, and external magnetic fields, several experiments have shown evidence of the formation of Majorana zero modes above a critical magnetic field [6–14].

In this work we propose a microscopic mechanism for the creation of Majorana zero modes in similar systems which occurs in the absence of spin-orbit interaction, magnetic fields, and superconductivity. Our mechanism relies simply on the interplay of the orbital physics of a nanowire with rotational symmetry and the three-dimensional Coulomb interaction. Our analysis contrasts with that of previous works investigating the role of interactions in Majorana systems in which induced superconductivity was essential [15–17]. We show that in nanowires with rotational symmetry, interactions involving finite angular momentum transfer between electrons (Fig. 1) create a strongly correlated phase with gaps appearing in the collective modes. In our system the electrons are fractionalized, and the elementary excitations each carry only a part of the original electronic degrees of freedom. A topological phase emerges within the sector associated with the product of the spin and orbital momentum, or *helicity*, $\chi = ls$, establishing the presence of Majorana edge modes. The possible destruction of the Luttinger liquid behavior due to the formation of gaps in some sectors of the excitation spectrum was first analyzed by Luther and Emery in quantum wires with attractive backscattering [18]; more recently, these phases have been investigated in coupled spinless chains [19–24], ultracold atoms with artificial spin-orbit coupling [25], and nanowires with commensurate Fermi and spin-orbit momenta [26], while interacting topological 1D models without the violation of fermion number conservation have also been explored in coupled superconducting nanowires [27] and 1D superfluid chains [28]. We note that Majorana fermions without superconductivity and in the absence of a nontrivial bulk topology appeared in Emery and Kivelson's earlier study of two-channel Kondo impurities [29].

Our system has characteristics phenomenologically similar to p-wave superconductors, namely, a gap to fermionic quasiparticle excitations which is visible in tunneling transport and a ground-state degeneracy due to the edge modes. However, our system exhibits Z_2 rather than continuous symmetry breaking, and the topological sector consists of condensate of emergent fractional fermions which are both spinless and neutral (as opposed to conventional superconductivity), and time-reversal symmetry is not lifted as is the case for p-wave superconductors.

II. MODEL HAMILTONIAN

We model the interacting nanowire by the three-dimensional Hamiltonian which includes the Coulomb interaction,

$$H = \sum_s \int \psi_s^\dagger(\boldsymbol{r})\left[\frac{\boldsymbol{p}^2}{2m^*} + V(x,y)\right]\psi_s(\boldsymbol{r})d^3\boldsymbol{r} + \frac{e^2}{2\epsilon_r}\sum_{s,s'}\int \frac{\psi_{s'}^\dagger(\boldsymbol{r}')\psi_s^\dagger(\boldsymbol{r})\psi_s(\boldsymbol{r})\psi_{s'}(\boldsymbol{r}')}{|\boldsymbol{r}-\boldsymbol{r}'|}d^3\boldsymbol{r}d^3\boldsymbol{r}', \quad (1)$$

where $V(x,y)$ is the 1D confining potential, which we assume possesses N-fold rotational symmetry. The single-electron states $|n,l,k,s\rangle$ possess a principal quantum number n indexing radial excitations, conserved momentum k along the wire axis, spin $s = \uparrow, \downarrow$, and angular momentum $l = 0, 1, \ldots, N-1$ associated with the phase $e^{2\pi i l/N}$ acquired

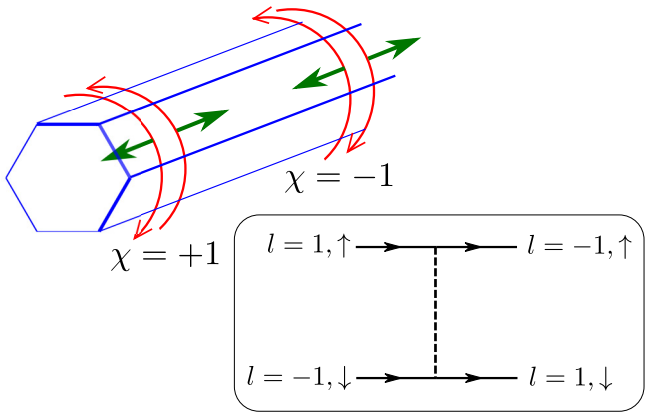

FIG. 1. A hexagonal wire, with electron orbital trajectories and spins (bold arrows) corresponding to positive and negative helicities χ. Inset: the angular momentum and spin structure of the central interaction driving the topological physics.

under $2\pi/N$ rotation. For $l \neq 0$, there is a double degeneracy between states with equal and opposite values of l, which are related by time reversal. In order to maximize the effect of interactions, we also suppose an experimental setup in which the electronic wave function is confined to a thin region on the surface of the nanowire (as is the case, for example, in a GaAs/AlGaAs core-shell nanowire [30,31]). The radial excitations then exist at much higher energy than the angular excitations in the cross section of the wire, and the lowest three 1D bands consist of states with $n = 0$, $l = 0, -1, 1$. We consider the situation where only these three orbital modes are occupied.

The Coulomb interaction connects initial and final two-electron states $|i\rangle = |k_1, l_1, s_1\rangle \otimes |k_2, l_2, s_2\rangle$ and $|f\rangle = |k_3, l_3, s_3\rangle \otimes |k_4, l_4, s_4\rangle$, and discrete rotational symmetry implies $l_1 + l_2 = l_3 + l_4$ mod N. For $N > 4$, the selection rules for interaction matrix elements are identical to those for a cylindrical wire ($N = \infty$), which is the case we shall consider. In addition to enforcing the angular momentum selection rules, the rotational symmetry of the wire also guarantees the degeneracy of the highest filled subbands. The matrix elements of the interaction term U [i.e., the second line in Eq. (1)], assuming the Coulomb interaction is long range, for $N > 4$ may be well approximated by those in a cylindrical wire and are given by

$$\langle f|U|i\rangle = \frac{2e^2}{\epsilon_r} I_{l_3-l_1}(qR) K_{l_3-l_1}(qR), \tag{2}$$

where I_j and K_j are the modified Bessel functions and $q = k_3 - k_1$ is the exchanged momentum. For the case of forward scattering ($q = 0$) with nonzero angular momentum transfer ($l_3 \neq l_1$), the interactions become $e^2/(\epsilon_r|l_3 - l_1|)$. For $l_3 = l_1$, expression (2) diverges logarithmically as $q \to 0$. Assuming the existence of a screening plane at distance $L \gg R$, these interactions are screened to the values $(2e^2/\epsilon_r)\ln(2L/R)$, which is $\approx 6.0e^2/\epsilon_r - 9.2e^2/\epsilon_r$ for $L/R = 10$–50.

III. RENORMALIZATION GROUP ANALYSIS

Concentrating on scattering processes close to the Fermi level (i.e., at momenta $k \approx \pm k_l$ equal to the Fermi momenta in the l bands), we find a total of 12 independent couplings, with six forward-scattering interactions, which we denote by $\Gamma_{l_1 l_2 l_3 l_4}$ with momentum transfer $k_{l_3} - k_{l_1}$, and six backscattering interactions $\hat{\Gamma}_{l_1 l_2 l_3 l_4}$ with momentum transfer $k_{l_1} + k_{l_3}$. In order to deal with the large number of competing interactions, we have calculated the running of the couplings under the renormalization group (RG), which reduces the number of interactions that become relevant at energy scales much lower than the Fermi energy.

The RG equations were obtained to second order in the couplings (see Appendix A) and solved numerically. We find that below a critical density $\epsilon_F < E^*$, where ϵ_F is the Fermi energy as measured from the edge of the $l = \pm 1$ bands, the density of states in the upper ($l = \pm 1$) bands is sufficiently larger than that in the lower ($l = 0$) band that the interaction between upper and lower bands becomes irrelevant. The value of the critical density depends weakly on the long-range interactions $U_{l_1 l_1 l_3 l_3}(q = 0) = (2e^2/\epsilon_r)\ln(2L/R)$; we have $E^* \approx 0.45E_L - 0.60E_L$ for $L/R = 10$–50, where $E_L = 1/2m^*R^2$ is the splitting between the upper and lower l bands. In the following we will consider only densities corresponding to $\epsilon_F < E^*$. In this case all interactions involving the upper bands flow to strong coupling.

IV. BOSONIZATION

Having observed from the RG solutions that only interactions involving the upper bands flow to strong coupling, we will hereafter focus on their description in terms of eight chiral modes labeled by $l = \pm 1$ and $s = \pm 1$ with right or left chirality $\mu = \pm 1$ corresponding to the sign of the velocity. We introduce a bosonized description [32] of the fermionic modes by expressing the fermionic fields as

$$\begin{aligned}\psi_{ls,\mu}(x) &= \sum_{\mu k - k_l < \Lambda/v_1} e^{ikx} c_{kls} \\ &= \sqrt{\Lambda/v_1}\exp\left\{\frac{i}{2}\left[\varphi_\rho^\mu(x)\right.\right. \\ &\quad \left.\left. + s\varphi_\sigma^\mu(x) + l\varphi_l^\mu(x) + ls\varphi_\chi^\mu(x)\right]\right\},\end{aligned} \tag{3}$$

where v_1 is the Fermi velocity in the $l = \pm 1$ bands and Λ is the running energy scale. The chiral bosonic fields $\partial_x \varphi_a^\mu$ represent the chiral densities of charge ($a = \rho$), orbital momentum ($a = l$), spin ($a = \sigma$), and helicity ($a = \chi$), with the latter being the difference between densities of electrons with angular momentum parallel to spin ($ls = 1$) and those with angular momentum antiparallel to spin ($ls = -1$). We note that the decomposition of four species of electrons into four bosonic fields is similar to Emery and Kivelson's analysis of the two-channel Kondo model [29]. We introduce the pairs of dual fields $\phi_a = \varphi_a^R - \varphi_a^L$ and $\theta_a = \varphi_a^R + \varphi_a^L$ satisfying $[\partial_x\theta_b(x'), \phi_a(x)] = 4\pi i\delta_{ab}\delta(x - x')$, which define the low-energy fluctuations of densities and currents, respectively, within each sector $a = \rho, l, \sigma, \chi$ of the excitation spectrum. The Hamiltonian density of the system is

given by

$$\mathcal{H} = \sum_{a=\rho,l,\sigma,\chi} \frac{v_a}{8\pi K_a}(\partial_x\phi_a)^2 + \frac{K_a v_a}{8\pi}(\partial_x\theta_a)^2 + 4\sum_{a,b=l,\sigma,\chi} G_{ab}\cos\phi_a\cos\phi_b + 4\sum_{a=l,\sigma}\widetilde{G}_a\cos\theta_\chi\cos\phi_a. \quad (4)$$

Here we have introduced the Luttinger parameters K_a and velocities v_a for each sector. The explicit relation between the running couplings Γ_{l_1,l_2,l_3,l_4}, $\hat{\Gamma}_{l_1,l_2,l_3,l_4}$ and the parameters K_a, v_a, G_{ab}, $\widetilde{G}_a$ of the sine-Gordon theory is provided in Appendix B.

Under the RG flow, K_ρ is fixed, $K_l, K_\sigma \to 0$, and $K_\chi \to \infty$. This implies that the interaction terms in Eq. (4) open a gap in the spin, orbital momentum, and helicity sectors, while the charge sector remains gapless. This scenario is similar to the one studied in Ref. [25] in the context of ultracold atoms with spin-orbit coupling. Concerning the spin and orbital sectors, only the fields ϕ_σ and ϕ_l are involved in the interaction terms. Hence these fields fluctuate around one of their semiclassical energy minima, giving rise to vacuum expectation values $\langle\cos\phi_\sigma\rangle \sim \langle\cos\phi_l\rangle \sim \pm 1$. The helicity sector presents instead both ϕ_χ and θ_χ interactions. Due to the flow of the Luttinger parameter $K_\chi \to \infty$, the θ_χ terms dominate; thus $\langle\cos\theta_\chi\rangle \sim \mp 1$, and hereafter, we will neglect the ϕ_χ interactions for the sake of simplicity. The signs of the real expectation values follow from those of the couplings, $G_{\sigma l} < 0$ and $\widetilde{G}_\sigma, \widetilde{G}_l > 0$ (see Appendix B).

In the strong-coupling limit, terms in the Hamiltonian (4) involving products of cosines may be decomposed in the mean-field approximation, which leads to the separation of the effective Hamiltonian into four sectors, $\mathcal{H} = \mathcal{H}_\rho + \mathcal{H}_\sigma + \mathcal{H}_l + \mathcal{H}_\chi$, where $\mathcal{H}_\rho$ describes the gapless charge modes and

$$\mathcal{H}_a = \frac{v_a K_a}{8\pi}(\partial_x\theta_a)^2 + \frac{v_a}{8\pi K_a}(\partial_x\phi_a)^2 + 4\sum_{b\neq a}[G_{ab}\langle\cos\phi_b\rangle + \widetilde{G}_a\langle\cos\theta_\chi\rangle]\cos\phi_a \quad (5)$$

for $a = \sigma, l$ and

$$\mathcal{H}_\chi = \frac{v_\chi K_\chi}{8\pi}(\partial_x\theta_\chi)^2 + \frac{v_\chi}{8\pi K_\chi}(\partial_x\phi_\chi)^2 + 4\sum_a\langle\cos\phi_a\rangle[G_{\chi a}\cos\phi_\chi + \widetilde{G}_a\cos\phi_\chi], \quad (6)$$

and we have neglected terms describing fluctuations of the cosines of the fields about their mean values.

V. PROPERTIES OF THE SYSTEM

In order to study the physical characteristics of the system, we may now introduce fermionic operators $\psi_{a,L}$, $\psi_{a,R}$ associated with the individual bosonic fields ϕ_a, θ_a appearing in the previous Hamiltonians. The mapping enforces the following relations between the vacuum expectation values of these fields:

$$\langle\cos\phi_a\rangle = \tfrac{1}{2}\langle\psi^\dagger_{a,R}\psi_{a,L} + \text{H.c.}\rangle, \quad (7)$$

$$\langle\cos\theta_\chi\rangle = \tfrac{1}{2}\langle\psi^\dagger_{\chi,R}\psi^\dagger_{\chi,L} + \text{H.c.}\rangle, \quad (8)$$

and the resulting effective Hamiltonians takes the form

$$\mathcal{H}_a = -iv_a[\psi^\dagger_{a,R}\partial_x\psi_{a,R} - \psi^\dagger_{a,L}\partial_x\psi_{a,L}] + U_a\psi^\dagger_{a,R}\psi_{a,R}\psi^\dagger_{a,L}\psi_{a,L} + \left[\sum_{b\neq a} G_{ab}\langle\psi^\dagger_{b,R}\psi_{b,L} + \text{H.c.}\rangle + \widetilde{G}_a\langle\psi^\dagger_{\chi,R}\psi^\dagger_{\chi,L} + \text{H.c.}\rangle\right](\psi^\dagger_{a,R}\psi_{a,L} + \text{H.c.}) \quad (9)$$

for $a = \sigma, l$ and

$$\mathcal{H}_\chi = -iv_\chi[\psi^\dagger_{\chi,R}\partial_x\psi_{\chi,R} - \psi^\dagger_{\chi,L}\partial_x\psi_{\chi,L}] + U_\chi\psi^\dagger_{\chi,R}\psi_{\chi,R}\psi^\dagger_{\chi,L}\psi_{\chi,L} + \sum_b\langle\psi^\dagger_{b,R}\psi_{b,L} + \text{H.c.}\rangle[G_{\chi b}\psi^\dagger_{\chi,R}\psi_{\chi,L} + \widetilde{G}_b\psi^\dagger_{\chi,R}\psi^\dagger_{\chi,L} + \text{H.c.}]. \quad (10)$$

The Hamiltonian densities contain mass terms proportional to $\psi^\dagger_{a,R}\psi_{a,L} + \text{H.c.}$ as well as $\psi^\dagger_{\chi,R}\psi^\dagger_{\chi,L} + \text{H.c.}$, describing particle-hole and particle-particle pairing, respectively. In addition, quartic interactions appear in all sectors which describe the fermionic self-interactions. For the σ and l fields, these self-interactions are repulsive ($U_\sigma, U_l > 0$), which corresponds to an attractive interaction between particles and holes which enhances the "excitonic" order parameter $\langle\psi^\dagger_R\psi_L\rangle$, while for the χ field, the self-interaction is attractive, $U_\chi < 0$, which enhances the "superconducting" order parameter $\langle\psi^\dagger_{\chi,R}\psi^\dagger_{\chi,L}\rangle$. It is therefore appropriate at the mean-field level to replace

$$\psi^\dagger_{a,R}\psi_{a,R}\psi^\dagger_{a,L}\psi_{a,L} \to -[\langle\psi^\dagger_{a,R}\psi_{a,L}\rangle\psi^\dagger_{a,L}\psi_{a,R} + \text{H.c.}] \quad (11)$$

for $a = \sigma, l$ and

$$\psi^\dagger_{\chi,R}\psi_{\chi,R}\psi^\dagger_{\chi,L}\psi_{\chi,L} \to \langle\psi^\dagger_{\chi,R}\psi^\dagger_{\chi,L}\rangle\psi_{\chi,L}\psi_{\chi,R} + \text{H.c.} \quad (12)$$

We then obtain expressions similar to the Bogoliubov–de Gennes Hamiltonians for excitonic and superconducting condensates,

$$\mathcal{H}_a = -iv_a[\psi^\dagger_{a,R}\partial_x\psi_{a,R} - \psi^\dagger_{a,L}\partial_x\psi_{a,L}] + \Delta_a(\psi^\dagger_{a,R}\psi_{a,L} + \text{H.c.}) \quad (13)$$

for $a = \sigma, l$ and

$$\mathcal{H}_\chi = -iv_\chi[\psi^\dagger_{\chi,R}\partial_x\psi_{\chi,R} - \psi^\dagger_{\chi,L}\partial_x\psi_{\chi,L}] + \Delta^E_\chi(\psi^\dagger_{\chi,R}\psi_{\chi,L} + \text{H.c.}) + \Delta^S_\chi(\psi^\dagger_{\chi,R}\psi^\dagger_{\chi,L} + \text{H.c.}), \quad (14)$$

where

$$\Delta_a = -U_a\langle\psi^\dagger_{a,R}\psi_{a,L}\rangle + 2\sum_{b\neq a} G_{ab}\langle\psi^\dagger_{b,R}\psi_{b,L}\rangle + 2\widetilde{G}_a\langle\psi^\dagger_{\chi,R}\psi^\dagger_{\chi,L}\rangle \tag{15}$$

for $a = \sigma, l$ and

$$\Delta^E_\chi = 2\sum_{a\neq\chi} G_{\chi a}\langle\psi^\dagger_{a,R}\psi_{a,L}\rangle,$$
$$\Delta^S_\chi = U_\chi\langle\psi^\dagger_{\chi,R}\psi^\dagger_{\chi,L}\rangle + 2\sum_a \widetilde{G}_a\langle\psi^\dagger_{a,R}\psi_{a,L}\rangle. \tag{16}$$

The gaps $\Delta_l, \Delta_\sigma, \Delta_\chi$ were determined from the self-consistency equations involving the coefficients $G_{ij}, \widetilde{G}_i$ (see Appendix B), which depend on the running couplings; however, the gaps may be calculated using any set of couplings along the RG trajectory in the strong-coupling regime: the running of the energy scale is compensated by the logarithmic enhancement of the couplings, and the system enters the strong-coupling regime when $\Lambda \approx \Delta_l \approx \Delta_\sigma \approx \Delta_\chi$. We therefore find that the resulting gaps are independent of the choice of Λ over the final portion of the RG flow. We note, however, that quantum fluctuations generated by irrelevant couplings suppress the gap during the initial stage of the RG flow; thus, to avoid overestimation of the gap, it is necessary to use renormalized couplings only after the irrelevant couplings have been eliminated.

The bulk excitation spectra in the $a = l, \sigma, \chi$ sectors are then given by

$$E_a = \pm\sqrt{v_a^2k^2 + \Delta_a^2}. \tag{17}$$

While we refer to the $\psi^\dagger_{R,a}\psi_{L,a}$ and $\psi^\dagger_{R,\chi}\psi^\dagger_{L,\chi}$ terms as excitonic and superconducting pairing interactions because they have the form of the pairing interactions occurring in the mean-field descriptions of excitonic and p-wave superconductors, respectively, it is crucial to note that the order parameters Δ_i consist of real expectation values $\langle\psi^\dagger_{a,R}\psi_{a,L} + \text{H.c.}\rangle$ and $\langle\psi^\dagger_{\chi,R}\psi^\dagger_{\chi,L} + \text{H.c.}\rangle$, which do not possess a complex phase, and thus there is no spontaneously broken U(1) symmetry, as required by the Mermin-Wagner theorem.

The gaps in the σ, l, χ sectors allow for the description of the system in terms of nearly free fermionic quasiparticles, with corrections to the free motion being suppressed by the gap. Unlike the original electrons, which each carry charge, spin, angular momentum, and helicity simultaneously, the true excitations each carry only one of these quantum numbers. We find that the Luttinger liquid behavior ordinarily expected for interacting quantum wires survives only in the gapless charge excitations. In the remaining sectors, operators pairing oppositely moving quasiparticles develop expectation values in the ground state, and we may describe the gapped sectors as condensed states of emergent, fractional fermions.

In the helicity sector, the superconducting term $\propto \psi^\dagger_{\chi R}\psi^\dagger_{\chi L}$ has a simple physical origin. The action of this product of fermionic operators is to locally change the helicity densities $\partial_x\phi_\chi$ without affecting the spin, charge, or orbital angular momentum. This originates from collisions involving angular momentum transfer with structure $\psi^\dagger_{-1\uparrow}\psi^\dagger_{1\downarrow}\psi_{1\uparrow}\psi_{-1\downarrow}$, in which one pair of positive-helicity ($l = s$) electrons is converted into one pair of negative-helicity ($l = -s$) electrons (see Fig. 1). This interaction connects quantum states in which the number of electrons of a certain helicity is raised by two. It is also simple to see why the superconducting term occurs only within the helicity sector: two-electron collisions in which either the total spin or the total angular momentum of the pair is changed are forbidden by symmetry. However, it is possible for either spin or angular momentum to be transferred between right- and left-moving electrons, and when expressed in terms of quasiparticle operators, such interactions take the form $\psi^\dagger_{l,R}\psi_{l,L}$ and $\psi^\dagger_{\sigma,R}\psi_{\sigma,L}$. It should also be noted that terms containing products $\psi^\dagger_{\chi,R}\psi_{\chi,L}$ are also present in the exact Hamiltonian, which correspond to the ϕ_χ interactions in Eq. (4); however, they are fully screened by the condensate, which is consistent with the running of $K_\chi \to \infty$ under RG. In the mean-field solution of (13) and (14) we find $\Delta_l = \Delta_\sigma = \Delta_\chi = \Delta$.

Solving the mean-field Hamiltonians for the emergent fermions (13) and (14) in the presence of boundary conditions corresponding to full reflection at the edges of the system yields zero-energy modes $\gamma_{a,1}$ ($\gamma_{a,2}$) localized to the left (right) of the system and decaying into the bulk with characteristic length $\xi = v_a/\Delta$. These edge modes have also been demonstrated in previous studies of topologically gapped strongly correlated systems [33–35]. In the helicity sector, the presence of the superconducting term implies that these edge modes are self-conjugate, $\gamma_{\chi,1} = \gamma^\dagger_{\chi,1}$ and $\gamma_{\chi,2} = \gamma^\dagger_{\chi,2}$, and therefore emergent Majorana fermions; for the spin and orbital sectors, instead, $\gamma^\dagger_{a,i} \neq \gamma_{a,i}$, and it is possible to define boundary occupation numbers $n_{l/\sigma,i} = \gamma^\dagger_{l/\sigma,i}\gamma_{l/\sigma,i}$. In total the system possesses a 32-fold ground-state degeneracy arising from the possible occupations of these four Dirac edge modes in the l and σ sectors, labeled by $n_{l/\sigma,i} = 0, 1$, and the Majorana fermionic parity $i\gamma_{\chi,1}\gamma_{\chi,2} = \pm 1$. We observe that the degeneracy obtained by the Dirac modes can be removed by the addition of arbitrarily small boundary terms, proportional to $n_{l/\sigma,i}$ and thus to the local spin or orbital density. Furthermore, as in similar models, disorder may cause a weak splitting of the degeneracy induced by the Majorana modes, with gaps decaying algebraically with the system size [17,34].

For the sake of simplicity, we derived the existence of the Majorana zero modes and the related degeneracy from the mean-field Hamiltonians (13) and (14). However, the same results can be obtained in a more rigorous framework from (4) by generalizing to our system the semiclassical analysis of the zero-energy edge modes in [36]. A further analysis of the ground-state degeneracy in interacting topological nanowires can be found in [17].

From Eq. (2), the bare values of the interactions $U_{l_1,l_2,l_3,l_4}(q) \sim e^2/\epsilon_r = g$, and the gap may be very crudely estimated via the mean-field expression

$$\Delta \sim \epsilon_F e^{-\frac{2\pi v_F}{g}} = \epsilon_F e^{-\sqrt{\frac{\epsilon_F}{E_g}}},$$
$$E_g = \frac{1}{4\pi^2}\frac{m^*e^4}{2\epsilon_r^2} \sim \frac{m^*/m_e}{4\pi^2\epsilon_r^2} \times 13.6\ \text{eV}, \tag{18}$$

where m^* is the effective mass in the semiconductor. The gap is enhanced in materials with larger effective mass. For GaAs,

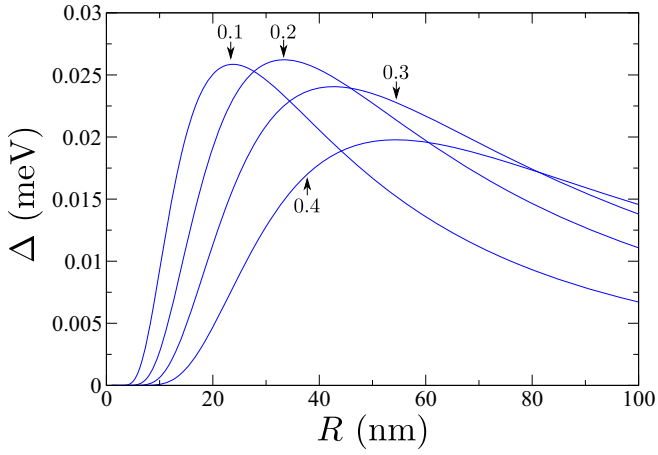

FIG. 2. Solid curves: the topological gap Δ (meV) as a function of the wire radius R for various values of the Fermi energy ϵ_F measured from the bottom of the upper bands, $\epsilon_F/E_L = 0.1, 0.2, 0.3, 0.4$. The material parameters for GaAs are used, $m^* = 0.067m_e$, $\epsilon_r = 12.9$.

$m^* = 0.067m_e$, and the gap is of the order of ϵ_F when $\epsilon_F \approx E_g \approx 0.14$ meV. The calculated values of the gap as a function of the ratio ϵ_F/E_L (where $E_L = 1/2m^*R^2$) for different values of R are plotted in Fig. 2. We find that the maximum value of the gap $\Delta \sim 0.025$ meV ≈ 0.3 K, which differs from the mean-field estimate by nearly a factor of 6. This suppression of the gap is due to the effect of quantum fluctuations which are accounted for in our second-order RG analysis. We observe that, while mean-field theory is accurate in the strong-coupling limit, we are required to use renormalized couplings generated by the second-order RG flow rather than bare couplings.

The existence of subgap edge states in the σ, l, and ξ sectors in combination with a gapless total charge mode has profound consequences on the tunneling transport characteristics of the system. The local density of states (LDOS) $A_{ls}(x,\omega)$ is a convolution of two-point correlation functions involving the gapless ρ field as well as the σ, l, and χ fields, which possess both gaps to continuum excitations and subgap states localized at the edges of the system. Expressing the LDOS in terms of the Matsubara Green's function

$$A_{ls}(x,\omega) = -\frac{1}{\pi}\mathrm{Im}\mathcal{G}_l(x,-i\omega), \tag{19}$$

where

$$\mathcal{G}_l(x,\omega) = -\int \mathcal{T}\langle\psi_{ls}(x,\tau)\psi^\dagger_{ls}(x,0)\rangle e^{i\omega\tau}d\tau, \tag{20}$$

we find that the gapless $l=0$ modes provide a power-law contribution which is well known in Luttinger liquid theory, while the contribution from the $l=\pm1$ bands is a product of the correlation functions in all sectors,

$$\mathcal{G}_{|l|=1}(x,\tau) = \mathrm{sgn}(\tau)g_\rho(x,\tau)g_\sigma(x,\tau)g_l(x,\tau)g_\chi(x,\tau). \tag{21}$$

Due to the edge modes appearing in the gapped sectors, the relative correlations consist of a τ-independent contribution κ arising from the zero-energy modes as well as a τ-dependent factor due to the continuum states:

$$\begin{aligned} g_\rho(\tau) &= |\tau|^{-\frac{\gamma}{4}}, \\ g_a(\tau) &= \kappa_a + |\tau|^{-\frac{1}{4}}e^{-\Delta_a|\tau|}, \quad a=\sigma,l,\chi, \end{aligned} \tag{22}$$

with $\gamma > 1$ being an interaction-dependent exponent. The constants κ_a are of order unity at the edge and decay exponentially as x moves into the bulk of the system. The calculation of γ is significantly complicated by the presence of interactions between the $l=0$ and $l=1$ states, which are marginal under the RG flow but nevertheless must be included because the charge sector is gapless. The full details of this calculation are presented in Appendix C.

Converting to the frequency representation, $G^R_{|l|=1}(x,\omega) = \mathcal{G}_{|l|=1}(x,-i\omega+0)$, we obtain the following expression for the LDOS:

$$\begin{aligned} -\frac{1}{\pi}\mathrm{Im}G^R_{|l|=1}(\omega) = {}& \frac{\kappa_l\kappa_\sigma\kappa_\chi}{\Gamma\left(\frac{\gamma}{4}\right)\Lambda^{\frac{\gamma}{4}-2}}|\omega|^{\frac{\gamma}{4}-1} + \kappa_l\kappa_\sigma\kappa_\chi\sum_i\frac{\Theta(|\omega|-\Delta_i)}{\kappa_i\Gamma\left(\frac{\gamma+1}{4}\right)\Lambda^{\frac{\gamma-7}{4}}}(|\omega|-\Delta_i)^{\frac{\gamma-3}{4}} \\ & + \kappa_l\kappa_\sigma\kappa_\chi\sum_{i<j}\frac{\Theta(|\omega|-\Delta_i-\Delta_j)}{\kappa_i\kappa_j\Gamma\left(\frac{\gamma+2}{4}\right)\Lambda^{\frac{\gamma-6}{4}}}(|\omega|-\Delta_i-\Delta_j)^{\frac{\gamma-2}{4}} + \frac{\Theta(|\omega|-\Delta_\sigma-\Delta_l-\Delta_\chi)}{\Gamma\left(\frac{\gamma+3}{4}\right)\Lambda^{\frac{\gamma-5}{4}}}(|\omega|-\Delta_\sigma-\Delta_l-\Delta_\chi)^{\frac{\gamma-1}{4}}, \end{aligned} \tag{23}$$

where $\Lambda = \Lambda_0 \approx \epsilon_F$ is the high-energy cutoff. The first term in the Green's function is proportional to $|\omega|^{\frac{\gamma}{4}-1}$ and exhibits a peak at zero frequency due to the fact that $\gamma < 4$ (see Appendix C). The remaining terms are defined for energies ω smaller than Δ_i, $\Delta_i+\Delta_j$, and $\Delta_\sigma+\Delta_l+\Delta_\chi$, corresponding to the gaps to various incoherent multi-Luther-Emery-fermion excitations.

The contribution to the LDOS from the upper bands $A_{l=\pm1,s}(x,\omega)$ is plotted in Fig. 3 for several values of R and ϵ_F/E_C and for varying distances x from an edge. We observe an algebraic peak at zero frequency, $A(x,\omega\approx0) = F(x)|\omega|^{-\gamma}$, with $F(x)$ decaying in the bulk of the system due to the localization of the zero-energy modes. This peak originates from the first term in Eq. (23). At $\omega \neq 0$, the LDOS clearly displays excitation bands emerging at energies $|\omega| > \Delta, 2\Delta, 3\Delta$, consistent with the other terms in Eq. (23).

The zero-frequency peak becomes narrower and eventually disappears at distances larger than the decay length of the edge modes, $x \gg \xi$, with $\xi = v_\chi/\Delta \approx 0.9$ μm for the parameters corresponding to Fig. 3. In the bulk of the system, the LDOS is vanishing for frequencies below the gaps, $|\omega| < \Delta$. Thus for certain distances along the wire, the tunneling density of states bears a striking resemblance to the zero-bias peak in Andreev reflection which has been observed several times

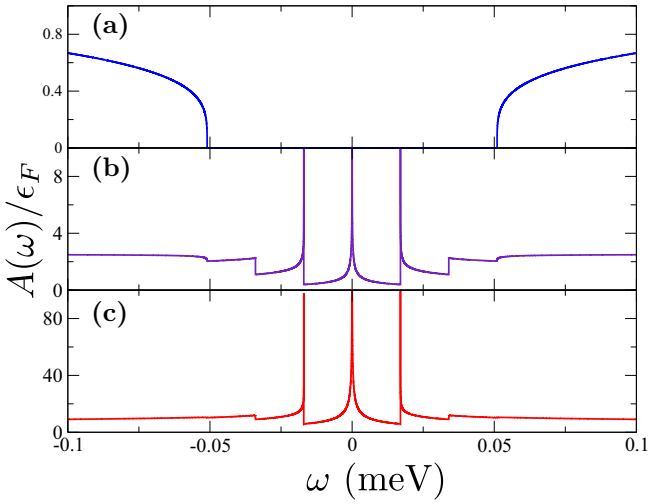

FIG. 3. The LDOS $A(x,\omega)$ for varying values of (a) $x/\xi = 10$, (b) 1, and (c) 0.1. Parameters are taken for a GaAs nanowire with $R = 25$ nm and $\epsilon_F = 0.3E_L$. Note that the scales on the vertical axes increase by an order of magnitude between each panel.

in superconducting nanowires [6–10,12–14], even though in our system superconductivity is absent. We also note that the structure of the LDOS is dramatically different from the one expected for a spinful Luttinger liquid, which always exhibits a power-law suppression at zero frequency, $A(x,\omega) \propto |\omega|^\gamma$, with $\gamma > 0$.

VI. CONCLUSIONS

We have presented a study of an interacting quantum wire with multiple degenerate orbitals occupied. The purely repulsive Coulomb interaction produces a strongly correlated phase which supports both gaps to collective excitations and a high ground-state degeneracy arising from zero-energy edge modes. We find a pair of Majorana fermions, as in 1D p-wave superconductors, despite the absence of superconductivity or, indeed, continuous symmetry breaking of any kind. Our mechanism relies on the degeneracy between the lowest pair of excited orbital states in a wire with N-fold discrete rotational symmetry. Performing a second-order RG analysis and approximating the bare interactions with those of a cylindrical wire, we have calculated the gaps to continuum excitations as well as the local density of states, which we find to exist at experimentally accessible energy scales. While our mechanism relies on rotational symmetry, we note that deviations from this symmetry will not destroy the Majorana fermions as long as the asymmetry-induced energy splitting is small compared to the size of the gaps.

Having focused on the physical properties of the Majorana modes, we have not explored ways in which they might be manipulated or how their non-Abelian nature might be demonstrated, which is of interest to future work. Since our system appears to be close to experimental realization, it is also an interesting prospect to investigate how alternative nanowire-based designs might also exhibit Majorana physics as a result of the intrinsic Coulomb interaction rather than relying on the spin-orbit interaction, magnetic fields, or superconductivity.

ACKNOWLEDGMENTS

The authors wish to acknowledge M. Leijnse, Y. Oreg, and P. Krogstrup for valuable discussions. M.B. acknowledges support from the Villum foundation. This work was supported by the Danish National Research Foundation.

APPENDIX A: SECOND-ORDER RG EQUATIONS

The vertices $\Gamma_{l_1l_2l_3l_4}$, $\hat{\Gamma}_{l_1l_2l_3l_4}$ are defined by matrix elements between two-electron states,

$$\langle f|U|i\rangle = \begin{cases} \Gamma_{l_1l_2l_3l_4}, & k_1,k_3>0, \quad k_2,k_4<0, \\ \hat{\Gamma}_{l_1l_2l_3l_4}, & k_1,k_4>0, \quad k_2,k_3<0, \end{cases}$$
$$|i\rangle = |k_1,l_1,s_1\rangle \otimes |k_2,l_2,s_2\rangle, \tag{A1}$$
$$|f\rangle = |k_3,l_3,s_3\rangle \otimes |k_4,l_4,s_4\rangle,$$

where U is the two-electron potential. In the following it will become convenient to introduce notation distinguishing four kinds of interactions,

$$U_{l_1l_2} = \Gamma_{l_1l_2l_1l_2}, \quad \tilde{U}_{l_1l_2} = \hat{\Gamma}_{l_1l_2l_2l_1},$$
$$V_1 = \Gamma_{0,0,1,-1}, \quad \tilde{V}_1 = \hat{\Gamma}_{0,0,1,-1}, \tag{A2}$$
$$V_2 = \Gamma_{1,-1,-1,1}, \quad \tilde{V}_2 = \hat{\Gamma}_{1,-1,1,-1},$$

so that $U_{l_1l_2}$ ($\tilde{U}_{l_1l_2}$) correspond to forward- (backward-) scattering interactions in which angular momentum is conserved for both left and right movers, while V_l ($\tilde{V}_l$) correspond to forward- (backward-) scattering interactions in which angular momentum $\pm l$ is transferred between the left- and right-moving densities.

Denoting

$$\lambda_0 = \frac{1}{2\pi v_0}, \quad \lambda_1 = \frac{1}{2\pi v_1}, \quad \lambda_{01} = \frac{1}{\pi(v_0+v_1)}, \tag{A3}$$

with v_0, v_1 being the Fermi velocities corresponding to the $l=0$ and $l=1$ bands, respectively, the flow of the couplings to second order are given by

$$\frac{dU_{11}}{dl} = \lambda_1\left[V_2^2 - \tilde{U}_{11}^2\right],$$
$$\frac{dU_{1,-1}}{dl} = -\lambda_1\left[V_2^2 + \tilde{V}_2^2 + \tilde{U}_{1,-1}^2\right],$$
$$\frac{dV_2}{dl} = 2\lambda_1[(U_{11}-U_{1,-1}) - \tilde{V}_2\tilde{U}_{1,-1}] - \lambda_0\left[V_1^2 + \tilde{V}_1^2\right],$$
$$\frac{dU_{00}}{dl} = -\lambda_0\tilde{U}_{00}^2 - 2\lambda_1\left[V_1^2 + \tilde{V}_1^2\right],$$
$$\frac{dU_{01}}{dl} = \lambda_{01}\left[V_1^2 - \tilde{U}_{01}^2\right],$$
$$\frac{dV_1}{dl} = -\lambda_0[U_{00}V_1 + \tilde{U}_{00}\tilde{V}_1] - \lambda_1[(U_{1,-1}+V_2)V_1 + (\tilde{V}_2 + \tilde{U}_{1,-1})\tilde{V}_1] + 2\lambda_{01}U_{01}V_1,$$
$$\frac{d\tilde{U}_{11}}{dl} = 2\lambda_1\left[\tilde{V}_2V_2 - \tilde{U}_{11}^2 - \tilde{V}_2^2\right],$$
$$\frac{d\tilde{V}_2}{dl} = 2\lambda_1[(U_{11}-U_{1,-1})\tilde{V}_2 + (\tilde{U}_{11}-\tilde{U}_{1,-1})V_2 - 2\tilde{U}_{11}\tilde{V}_2] - 2\lambda_0V_1\tilde{V}_1,$$

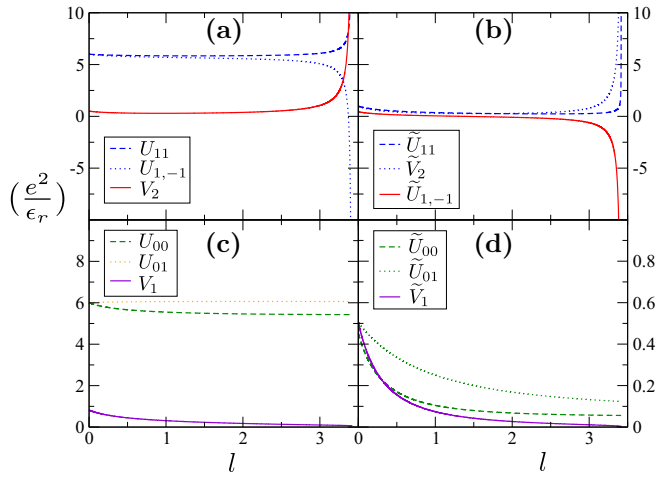

FIG. 4. The second-order RG flow of the interactions (A2), with bare parameters corresponding to a GaAs nanowire with $R = 25$ nm and $\epsilon_F = 0.3E_L$. (a) and (b) show interactions that involve only the $l = \pm 1$ bands, which flow to strong coupling. (a) and (c) show forward-scattering interactions, while (b) and (d) show backscattering interactions. Note that the scales on the axes in (a) and (b) and those in (c) and (d) are different.

$$
\begin{aligned}
\frac{d\widetilde{U}_{1,-1}}{dl} &= -2\lambda_1\left[V_2\widetilde{V}_2 + \widetilde{U}_{1,-1}^2\right] - 2\lambda_0 V_1\widetilde{V}_1,\\
\frac{d\widetilde{U}_{00}}{dl} &= -2\lambda_0\widetilde{U}_{00}^2 - 4\lambda_1 V_1\widetilde{V}_1,\\
\frac{d\widetilde{U}_{01}}{dl} &= 2\lambda_{01}\left[V_1\widetilde{V}_1 - \widetilde{U}_{01}^2 - \widetilde{V}_1^2\right],\\
\frac{d\widetilde{V}_1}{dl} &= -\lambda_0[U_{00}\widetilde{V}_1 + \widetilde{U}_{00}V_1]\\
&\quad - \lambda_1[V_1\widetilde{V}_2 + V_1\widetilde{U}_{1,-1} + \widetilde{V}_1 U_{1,-1} + \widetilde{V}_1 V_2]\\
&\quad + 2\lambda_{01}[\widetilde{V}_1 U_{01} + \widetilde{U}_{01}V_1 - 2\widetilde{U}_{01}\widetilde{V}_1].
\end{aligned}
\tag{A4}
$$

The solution of the RG equations (A4) with initial couplings corresponding to a GaAs nanowire ($m^* = 0.067m_e$, $\epsilon_r = 12.9$) with $R = 25$ nm and $\epsilon_F = 0.3E_L$ is plotted in Fig. 4. The plots show that the six interactions involving the $l = \pm 1$ bands $U_{11}, U_{1,-1}, V_2, \widetilde{U}_{11}, \widetilde{U}_{1,-1}, \widetilde{V}_2$ flow to strong coupling, while U_{00}, U_{01} remain marginal. The remaining interactions are irrelevant.

APPENDIX B: TECHNICAL DETAILS ON BOSONIZATION AND REFERMIONIZATION

Following the notation of Appendix A, the parameters of the bosonic Hamiltonian densities (4) are related to the bare fermionic interactions by

$$
\begin{aligned}
v_\sigma &= v_1 + \frac{V_2^{(0)}}{2\pi}, \quad v_l = v_1 - \frac{V_2^{(0)}}{2\pi}, \quad v_\chi = v_1 - \frac{V_2^{(0)}}{2\pi},\\
K_a &= \sqrt{\frac{\widetilde{v}_a - U_a/2\pi}{\widetilde{v}_a + U_a/2\pi}},\\
U_\sigma &= -\widetilde{U}_{11} - \widetilde{U}_{1,-1},\\
U_l &= 2U_{11} - 2U_{1,-1} - \widetilde{U}_{11} + \widetilde{U}_{1,-1},\\
U_\chi &= -\widetilde{U}_{11} + \widetilde{U}_{1,-1},\\
G_{l\sigma} &= -\widetilde{V}_2, \quad G_{\sigma\chi} = -\widetilde{U}_{11}, \quad G_{l\chi} = V_2 - \widetilde{V}_2,\\
\widetilde{G}_l &= V_2, \quad \widetilde{G}_\sigma = -\widetilde{U}_{1,-1},
\end{aligned}
\tag{B1}
$$

with $V_2^{(0)}$ being the bare (unrenormalized) value of V_2.

The mean-field Hamiltonians (13) and (14) in the main text may be easily solved in the limit $\Delta_\sigma, \Delta_l \ll \epsilon_F$ and either $\Delta_\chi^E \ll \epsilon_F$ or $\Delta_\chi^S \ll \epsilon_F$, yielding

$$
\begin{aligned}
\langle\psi_{a,R}^\dagger\psi_{a,L}\rangle &= -\frac{\Delta_a}{2\pi v_i}\ln\frac{2\Lambda}{|\Delta_a|}, \quad a = \sigma, l,\\
\langle\psi_{\chi,R}^\dagger\psi_{\chi,L}\rangle &= -\frac{1}{4\pi v_\chi}\left[\Delta_+\ln\frac{2\Lambda}{|\Delta_+|} - \Delta_-\ln\frac{2\Lambda}{|\Delta_-|}\right],\\
\langle\psi_{\chi,R}^\dagger\psi_{\chi,L}^\dagger\rangle &= -\frac{1}{4\pi v_\chi}\left[\Delta_+\ln\frac{2\Lambda}{|\Delta_+|} + \Delta_-\ln\frac{2\Lambda}{|\Delta_-|}\right],\\
\Delta_\pm &= \Delta_\chi^S \pm \Delta_\chi^E.
\end{aligned}
\tag{B2}
$$

Assuming $\Delta_\sigma \sim \Delta_l \sim \Delta_\pm \sim \Delta$, we may approximate the logarithmic factors by $\ln(\Lambda/\Delta)$ and $v_l, v_\chi, v_\sigma \approx v_F$ (assuming $V_2^{(0)} \ll 2\pi v_F$), which yields the mean-field equations

$$
\begin{pmatrix}\Delta_\sigma\\ \Delta_l\\ \Delta_\chi^S\\ \Delta_\chi^E\end{pmatrix} = -\frac{1}{2\pi v_F}\ln\frac{2\Lambda}{\Delta}
\times \underbrace{\begin{pmatrix} -U_\sigma & 2G_{\sigma l} & 2\widetilde{G}_\sigma & 2G_{\sigma\chi}\\ 2G_{\sigma l} & -U_l & 2\widetilde{G}_l & 2G_{l\chi}\\ 2\widetilde{G}_\sigma & 2\widetilde{G}_l & U_\chi & 0\\ 2G_{\sigma\chi} & 2G_{l\chi} & 0 & 0\end{pmatrix}}_{\boldsymbol{G}}
\begin{pmatrix}\Delta_\sigma\\ \Delta_l\\ \Delta_\chi^S\\ \Delta_\chi^E\end{pmatrix}.
\tag{B3}
$$

Denoting the largest negative eigenvalue of $\boldsymbol{G}$ by λ, the gap is then given by

$$
\Delta = 2\Lambda e^{\frac{2\pi v_F}{\lambda}} = 2\Lambda e^{-\frac{2\pi v_F}{|\lambda|}}.
\tag{B4}
$$

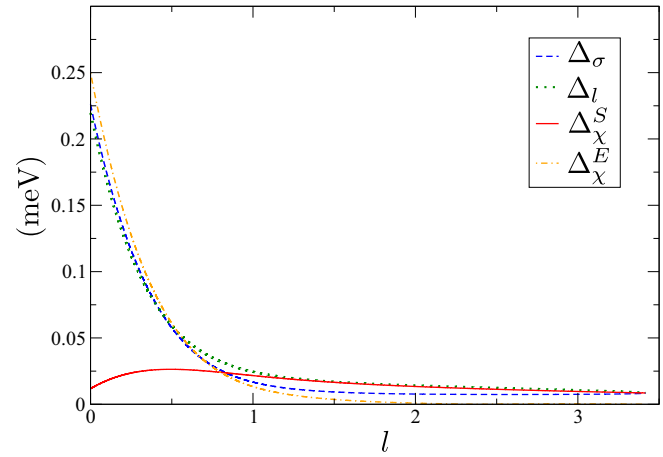

FIG. 5. The mean-field solution for the gaps Δ_σ (blue dashed line), Δ_l (green dotted line), Δ_χ^S (red solid line), and Δ_χ^E (orange dash-dotted line). Parameters correspond to a GaAs nanowire with $R = 25$ nm and $\epsilon_F = 0.3E_l$.

Since the RG flows exhibit a divergence at a finite scale $l = l^*$, the gap is also equal to

$$\Delta = 2\Lambda_0 e^{-l^*} \approx 2\epsilon_F e^{-l^*}. \tag{B5}$$

The solution of the mean-field equations (B3) for a GaAs nanowire with $R = 25\,\text{nm}$ and $\epsilon_F = 0.3E_l = 0.26\,\text{meV}$ is shown as a function of the running scale in Fig. 5. Applying mean-field theory with the bare interactions ($l = 0$), we find that gaps exist in all sectors, with $|\Delta_\sigma|, |\Delta_l|, |\Delta^E_\chi| \gg |\Delta^S_\chi| \approx 0.25\,\text{meV}$. Under the RG flow, we find that $\Delta^E_\chi \to 0$ and the remaining gaps converge to a value $\approx 0.017\,\text{meV}$. This shows that second-order RG is necessary to resolve the competition between the excitonic and superconducting orders in the χ sector.

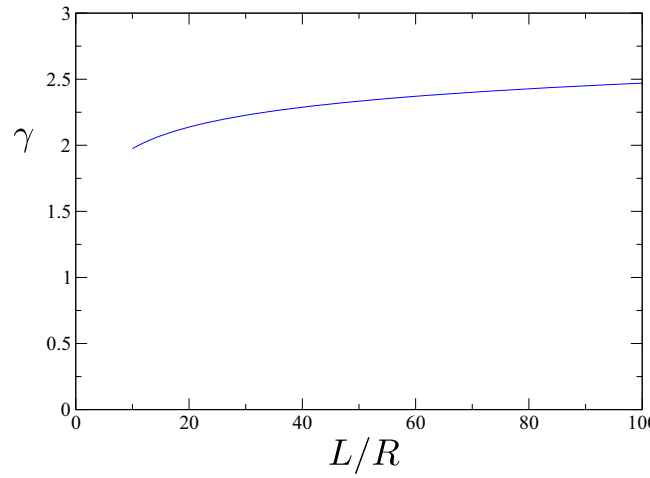

FIG. 6. Calculated values of the exponent γ appearing in Eq. (22) as a function of the ratio L/R, where L is the distance to the screening plane and R is the radius of the wire.

APPENDIX C: CALCULATION OF THE EXPONENT γ

The Hamiltonian density in the charge sector is

$$\mathcal{H} = \frac{1}{4\pi}\left[\left(v_0 + \frac{U_{00}}{\pi}\right)\left(\partial_x\varphi^R_{\rho^0}\right)^2 + \left(v_1 + \frac{2U_{11} + 2U_{1,-1} + V_2}{2\pi}\right)\left(\partial_x\varphi^R_{\rho^+}\right)^2 + \frac{2\sqrt{2}U_{01}}{\pi}\partial_x\varphi^R_{\rho^0}\partial_x\varphi^R_{\rho^+} + R \to L\right]$$
$$- \frac{1}{4\pi^2}\left\{(2U_{00} - \widetilde{U}_{00})\partial_x\varphi^R_{\rho^0}\partial_x\varphi^L_{\rho^0} + (2U_{11} + 2U_{1,-1} - \widetilde{U}_{11} - \widetilde{U}_{1,-1})\partial_x\varphi^R_{\rho^+}\partial_x\varphi^L_{\rho^+} + 2\sqrt{2}U_{01}\left[\partial_x\varphi^R_{\rho^0}\partial_x\varphi^L_{\rho^+} + L \leftrightarrow R\right]\right\}, \tag{C1}$$

where the fields

$$\varphi^R_{\rho^+} = \frac{\varphi^R_{l=1,\uparrow} + \varphi^R_{l=1,\downarrow} + \varphi^R_{l=-1,\uparrow} + \varphi^R_{l=-1,\downarrow}}{2},$$
$$\varphi^R_{\rho^0} = \frac{\varphi^R_{l=0,\uparrow} + \varphi^R_{l=0,\downarrow}}{\sqrt{2}} \tag{C2}$$

and $\uparrow, \downarrow$ are the spin indices. The interactions are given by

$$U_{l_1 l_2} = \frac{2e^2}{\epsilon_r}\ln\frac{2L}{R} = U_0, \quad \widetilde{U}_{ll} = \frac{2e^2}{\epsilon_r}I_0(2k_l R)K_0(2k_l R),$$
$$\widetilde{U}_{1,-1} = \frac{2e^2}{\epsilon_r}I_2(2k_1 R)K_2(2k_1 R), \tag{C3}$$

where R is the radius of the wire, k_l are the Fermi momenta in bands $l = 0, \pm 1$, and $L \gg R$ is the distance to the nearest screening plane.

The Hamiltonian density must be diagonalized via canonical transformation, which gives

$$\mathcal{H} = \sum_{\gamma=1,2}\frac{v_\gamma}{4\pi}\left[\left(\partial_x\widetilde{\varphi}^R_\gamma\right)^2 + \left(\partial_x\widetilde{\varphi}^L_\gamma\right)^2\right], \tag{C4}$$

where

$$\partial_x\widetilde{\varphi}^R_\gamma = \sum_\alpha U^\alpha_\gamma\partial_x\varphi^R_\alpha - V^\alpha_\gamma\partial_x\varphi^L_\alpha,$$
$$\partial_x\widetilde{\varphi}^L_\gamma = \sum_\alpha -V^\alpha_\gamma\partial_X\varphi^R_\alpha + U^\alpha_\gamma\partial_x\varphi^L_\alpha,$$
$$\alpha = (\rho^0, \rho^+), \tag{C5}$$

and the coefficients satisfy

$$\begin{pmatrix} 2\pi v_0 + 2U_0 & 2\sqrt{2}U_0 & -2U_0 + \widetilde{U}_{00} & -2\sqrt{2}U_0 \\ 2\sqrt{2}U_0 & 2\pi v_1 + 4U_0 + V_2 & -2\sqrt{2}U_0 & -4U_0 + \widetilde{U}_{11} + \widetilde{U}_{1,-1} \\ 2U_0 - \widetilde{U}_{00} & 2\sqrt{2}U_0 & -2\pi v_0 - 2U_0 & -2\sqrt{2}U_0 \\ 2\sqrt{2}U_0 & 4U_0 - \widetilde{U}_{11} - \widetilde{U}_{1,-1} & -2\sqrt{2}U_0 & -2\pi v_1 - 4U_0 - V_2 \end{pmatrix} \begin{pmatrix} U_\gamma^{\rho^0} \\ U_\gamma^{\rho^+} \\ V_{\gamma,\rho^0} \\ V_\gamma^{\rho^+} \end{pmatrix} = 2\pi v_\gamma \begin{pmatrix} U_\gamma^{\rho^0} \\ U_\gamma^{\rho^+} \\ V_\gamma^{\rho^0} \\ V_\gamma^{\rho^+} \end{pmatrix}, \tag{C6}$$

with $v_\gamma > 0$.

Since $\widetilde{\varphi}_\gamma^R, \widetilde{\varphi}_\gamma^L$ are free fields, their correlation functions are given by

$$\left\langle e^{i\kappa[\varphi_\gamma^R(x,\tau) - \widetilde{\varphi}_\gamma^R(x,0)]} \right\rangle = \left\langle e^{i\kappa[\varphi_\gamma^L(x,\tau) - \widetilde{\varphi}_\gamma^L(x,0)]} \right\rangle = \frac{1}{|\tau|^{\kappa^2}}. \tag{C7}$$

The correlation function

$$\left\langle e^{\frac{i}{2}[\varphi_{\rho^+}^R(x,\tau) - \varphi_{\rho^+}^R(x,0)]} \right\rangle = \frac{1}{|\tau|^{\frac{\gamma}{4}}} \tag{C8}$$

may then be calculated straightforwardly by transformation from the $\varphi_{\rho^+}^R, \varphi_{\rho^0}^R$ fields to the free bosonic fields. γ is plotted as a function of L/R in Fig. 6. We obtain $\gamma \approx 2$–3 in the range $10 < L/R < 100$.

[1] G. E. Volovik and V. M. Yakovenko, J. Phys.: Condens. Matter **1**, 5263 (1989).
[2] N. Read and D. Green, Phys. Rev. B **61**, 10267 (2000).
[3] A. Y. Kitaev, Phys. Usp. **44**, 131 (2001).
[4] R. M. Lutchyn, J. D. Sau, and S. Das Sarma, Phys. Rev. Lett. **105**, 077001 (2010).
[5] Y. Oreg, G. Refael, and F. von Oppen, Phys. Rev. Lett. **105**, 177002 (2010).
[6] A. Das, Y. Ronen, Y. Most, Y. Oreg, M. Heiblum, and H. Shtrikman, Nat. Phys. **8**, 887 (2012).
[7] M. T. Deng, C. L. Yu, G. Y. Huang, M. Larsson, P. Caroff, and H. Q. Xu, Nano. Lett. **12**, 6414 (2012).
[8] V. Mourik, K. Zuo, S. M. Frolov, S. R. Plissard, E. P. A. M. Bakkers, and L. P. Kouwenhoven, Science **336**, 1003 (2012).
[9] A. D. K. Finck, D. J. Van Harlingen, P. K. Mohseni, K. Jung, and X. Li, Phys. Rev. Lett. **110**, 126406 (2013).
[10] M. T. Deng, S. Vaitiekėnas, E. B. Hansen, J. Danon, M. Leijnse, K. Flensberg, J. Nygård, P. Krogstrup, and C. M. Marcus, Science **354**, 1557 (2016).
[11] S. M. Albrecht, A. P. Higginbotham, M. Madsen, F. Kuemmeth, T. S. Jespersen, J. Nygård, P. Krogstrup, and C. M. Marcus, Nature (London) **531**, 206 (2016).
[12] F. Nichele, A. C. C. Drachmann, A. M. Whiticar, E. C. T. O'Farrell, H. J. Suominen, A. Fornieri, T. Wang, G. C. Gardner, C. Thomas, A. T. Hatke, P. Krogstrup, M. J. Manfra, K. Flensberg, and C. M. Marcus, Phys. Rev. Lett. **119**, 136803 (2017).
[13] O. Gül, H. Zhang, J. D. S. Bommer, M. W. A. de Moor, D. Car, S. R. Plissard, E. P. A. M. Bakkers, A. Geresdi, K. Watanabe, T. Taniguchi, and L. P. Kouwenhoven, Nat. Nanotechnol. **13**, 192 (2018).
[14] H. Zhang, C.-X. Liu, S. Gazibegovic, D. Xu, J. A. Logan, G. Wang, N. van Loo, J. D. S. Bommer, M. W. A. de Moor, D. Car, R. L. M. Op het Veld, P. J. van Veldhoven, S. Koelling, M. A. Verheijen, M. Pendharkar, D. J. Pennachio, B. Shojaei, J. S. Lee, C. J. Palmstrøm, E. P. A. M. Bakkers, S. D. Sarma, and L. P. Kouwenhoven, Nature (London) **556**, 74 (2018).
[15] E. M. Stoudenmire, J. Alicea, O. A. Starykh, and M. P. A. Fisher, Phys. Rev. B **84**, 014503 (2011).
[16] S. Gangadharaiah, B. Braunecker, P. Simon, and D. Loss, Phys. Rev. Lett. **107**, 036801 (2011).
[17] L. Fidkowski, R. M. Lutchyn, C. Nayak, and M. P. A. Fisher, Phys. Rev. B **84**, 195436 (2011).
[18] A. Luther and V. J. Emery, Phys. Rev. Lett. **33**, 589 (1974).
[19] M. Cheng and H.-H. Tu, Phys. Rev. B **84**, 094503 (2011).
[20] C. V. Kraus, M. Dalmonte, M. A. Baranov, A. M. Läuchli, and P. Zoller, Phys. Rev. Lett. **111**, 173004 (2013).
[21] N. Lang and H. P. Büchler, Phys. Rev. B **92**, 041118(R) (2015).
[22] F. Iemini, L. Mazza, D. Rossini, R. Fazio, and S. Diehl, Phys. Rev. Lett. **115**, 156402 (2015).
[23] K. Guther, N. Lang, and H. P. Büchler, Phys. Rev. B **96**, 121109(R) (2017).
[24] E. Cornfeld and E. Sela, Phys. Rev. B **92**, 115446 (2015).
[25] F. Iemini, L. Mazza, L. Fallani, P. Zoller, R. Fazio, and M. Dalmonte, Phys. Rev. Lett. **118**, 200404 (2017).
[26] Y. Oreg, E. Sela, and A. Stern, Phys. Rev. B **89**, 115402 (2014).
[27] J. D. Sau, B. I. Halperin, K. Flensberg, and S. Das Sarma, Phys. Rev. B **84**, 144509 (2011).
[28] G. Ortiz, J. Dukelsky, E. Cobanera, C. Esebbag, and C. Beenakker, Phys. Rev. Lett. **113**, 267002 (2014).
[29] V. J. Emery and S. Kivelson, Phys. Rev. B **46**, 10812 (1992).
[30] M. J. Tambe, L. F. Allard, and S. Gradečak, J. Phys.: Conf. Ser. **209**, 012033 (2010).
[31] J. L. Boland *et al.*, Nano Lett. **15**, 1336 (2015).
[32] T. Giamarchi, *Quantum Physics in One Dimension*, International Series of Monographs on Physics (Clarendon, Oxford, 2003).
[33] J. von Delft and H. Schoeller, Ann. Phys. (Berlin, Ger.) **7**, 225 (1998).
[34] J. Ruhman, E. Berg, and E. Altman, Phys. Rev. Lett. **114**, 100401 (2015).
[35] A. Montorsi, F. Dolcini, R. C. Iotti, and F. Rossi, Phys. Rev. B **95**, 245108 (2017).
[36] D. J. Clarke, J. Alicea, and K. Shtengel, Nat. Commun. **4**, 1348 (2013).